Electronic Supplementary Information (ESI)

Microfluidics-assisted synthesis and functionalization of monodisperse colloidal hydrogel particles for optomechanical biosensors

David Rettke[1], Christian Danneberg[1], Talika Alina Neuendorf[2], Sebastian Kühn[3], Jens Friedrichs[3], Nicolas Hauck[2], Carsten Werner[3], Julian Thiele[2,4], Tilo Pompe[1,3,*]

1) Institute of Biochemistry, Leipzig University, Johannisallee 21 – 23, 04103 Leipzig, Germany

2) Leibniz-Institut für Polymerforschung Dresden e.V., Hohe Strasse 6, 01069 Dresden, Germany

3) Leibniz-Institut für Polymerforschung Dresden e.V., Max Bergmann Center of Biomaterials, Hohe Strasse 6, 01069 Dresden, Germany

4) Dresden Center for Intelligent Materials (DCIM), Technische Universität Dresden, 01069 Dresden, Germany

* Corresponding Author:

Institute of Biochemistry, Leipzig University, Johannisallee 21 – 23, 04103 Leipzig, Germany

E-mail: tilo.pompe@uni-leipzig

S1. Current state and limits of SCP biosensing approaches based on PEG-hydrogel microparticles

In this context of hydrogel-based biosensing approaches, Pussak et al. introduced an optomechanical biosensor for the quantification of carbohydrates using the contact mechanics of micrometer-sized elastic hydrogel particles referred to as soft colloidal probes (SCP) [1]. The interface contact mechanics of colloidal particles is well established to describe the interaction forces between spherical particles and a spherical or planar surface. Contact mechanics models allow the interface interaction energy, the contact area and the mechanical particle deformation to relate to each other, as shown by the Johnson-Kendall-Roberts (JKR) model of elastic contact of attractive interactions, i.e. adhesion between the interface of a soft sphere and a rigid surface. Following **eq. 1**, the radius of contact area a can be related to the adhesion energy of a soft spherical probe and a hard surface W, whereby R is the radius of the SCP and E_{eff} is the effective elastic modulus of the probe ($E_{eff} = 4E / (3(1-\nu^2))$; E - Young's modulus, ν - Poisson ratio).

$$a^3 = 6\pi \frac{W}{E_{eff}} R^2 \quad (1)$$

Equipping SCP and planar surface with molecules of interest, in turn, permits to conveniently correlate the extent of interactions between the tethered moieties to the resulting contact area. So far, this approach has been adapted to measure non-specific and specific interactions in various applications ranging from adhesion between whole cells and ligands of cell surface receptors, probing interactions between biomolecules and synthetic polymers as well as to develop biosensors as the aforementioned carbohydrate sensor and for highly sensitive pM detection of glyphosate as well as estrogenic compounds [1–5]. A general description of competitive and direct binding assays employing SCPs as adhesion probes is presented in **Fig. S1.** The superior flexibility in target panel modification, multiplexing capacity, miniaturization capabilities and various adhesive contact readout technologies, i.e. on-site analysis, promise to build a platform for label-free, sensitive and selective detection of a wide range of analytes of significant importance in biomedical diagnostics and environmental monitoring in a cost- and time-efficient manner.

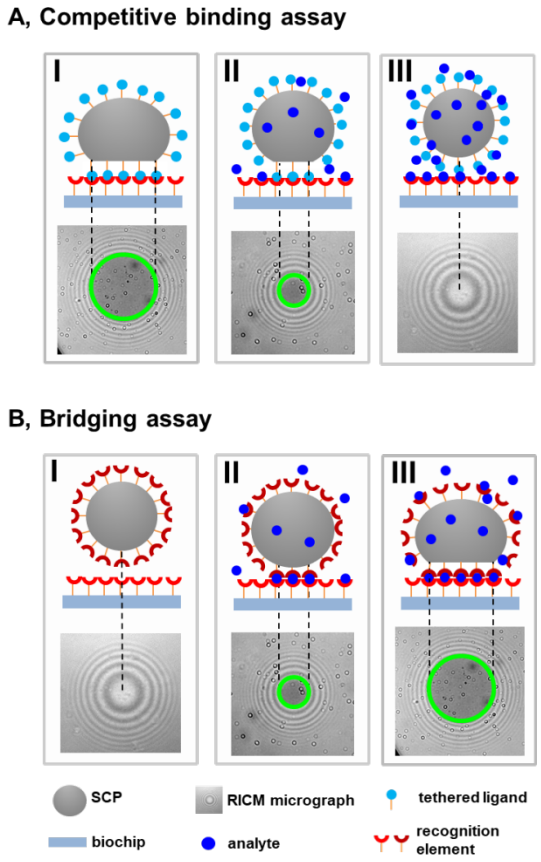

Figure S1: Schematic illustration of SCP-based biosensing assays. A, Competitive binding assay: **I,** An SCP equipped with ligands adheres to a transparent biochip bearing immobilized complementary receptors and forms an extended interfacial area as a result of biospecific interactions. **II,** Analytes present in the sample block binding sites for SCP tethered ligands. As a result, the contact area between SCP and biochip is markedly diminished. **III,** At high concentrations of analytes, the presented receptors are completely occupied, and the SCP cannot adhere to the biochip anymore. **B,** Bridging assay: SCP and biochip are decorated with receptors capable of binding to different domains of the analyte. **I,** In the absence of analytes, no biospecific interaction between SCP and biochip is observable, and no contact area is formed. **II** and **III,** Analytes within the sample to be analyzed cause a concentration-dependent increase in SCP-biochip interactions and contact area.

At present, SCPs for the aforementioned biosensing application are typically made of polyethylene glycol (PEG), which ensures a high degree of hydration, an almost ideally elastic hydrogel material, and a density equal to the surrounding aqueous media to avoid unspecific deformation of the particles. Furthermore, the inert and repellant nature of PEG aids to prevent any adhesion that does not result from the interactions between the molecules tethered to the surface and SCP. Previously, the synthesis of SCPs was carried out in a batch precipitation polymerization process using a kosmotropic salt to force aggregation of linear PEG diacrylate forming a dispersion followed by photoradical crosslinking of the end groups [4, 6–8]. Batch synthesis by this kind of precipitation polymerization is inevitably associated with a

comparatively broad distribution of particle size, a fact that complicates the analysis of the data obtained from adhesion experiments, application of alternative readout technologies, multiplexing and miniaturization. In particular, the SCP radius *R* has to be recorded together with the contact radius *a* in the case of polydisperse particles (see **eq. 1**), consuming resources for high-resolution optical instrumentation as well as image acquisition and data evaluation. Depending on the miniaturization setup and readout technology, only particles within a certain size can be taken into account for measurements. The lower limit for interferometric and holographic readouts, respectively, used in practice is typically limited to the resolution of the optical device, and smaller particles might lead to increasingly imprecise results. On the other hand, very large particles are prone to form irregular, non-circular contact areas, implying that simple physical models like the JKR approach are no longer applicable. Moreover, sets of defined particles in a narrow range of sizes, provides new opportunities for multiplexed analysis. Lastly, the batch process of precipitation polymerization of SCPs described above results in a certain percentage of particles with micrometer-sized defects due to the inclusion of kosmotrope solution droplets within the PEG-rich phase due to vigorous shaking of the reaction mixture prior crosslinking of the macromonomers. Overall, current SCP synthesis approaches results in a significant proportion of particles that are unsuitable for high-sensitivity quantification of adhesion energy and analytes, thus hindering further extension of SCP biosensing assays into a platform technology.

S2. Choice of materials and coupling reactions and ovierview on synthesized SCPs

Elasticity is a key feature of SCPs and the elastic modulus is determined by the precursor material, the solid content of the precursor material used for the synthesis, the particular architecture of the precursor molecule and the reactivity of the functional groups for cross-linking, i.e. the degree of conversion and resulting crosslinking density. As mentioned within the introduction, the lateral resolution of reflection interference contrast microscopy, which determines the accuracy with which the contact area is determined, is set by the limits of conventional optical microscopy and hence, contact areas of adhering SCPs should be larger than 1 µm in diameter [9]. Furthermore, the contact area must be spherical to assure applicability of JKR-model, whereby very soft SCPs with an elastic modulus below 10 kPa are prone to form large and irregular contact areas and high elastic moduli reduce the size of the resulting contact

area, thereby decreasing the sensitivity of the assays. Consequently, elastic moduli of SCPs of 20-40 kPa, which yield contact diameters of 1 µm or more with well-defined circular areas, are demanded [6]. In addition, offsets, i.e. the formation of contact areas in the absence of adhesion, should be avoided, as unspecific deformation of SCPs decreases the sensitivity of the respective assays for geometrical reasons.

PEG-based hydrogels can be prepared by chain-growth polymerization using vinyl-modified PEGs and a radical initiator. In addition, several strategies for preparing PEG-based hydrogels by a step-growth mechanism, leading to more homogeneous gels, were proposed and extensively exploited [10]. Chain-growth-polymerized PEG hydrogels are formed by propagation of active centers, i.e. free radicals, through unsaturated carbon-carbon bonds of the PEG macromonomers, whereas step-growth-polymerized PEG hydrogels are formed by at least two mutually reactive multifunctional macromonomers with an average macromonomer functionality greater than two [10-12]. For our studies, we used different linear as well as a star-shaped four-arm acrylamide-terminated PEGs, all of which are prepared according to the chain-growth mechanism. Low molecular weight PEGs, in this case 0.3 kDa, contribute more functional groups than high molecular weight PEGs, in this case 3.7 kDa at constant solid content. An increased number of functional groups should increase the crosslinking density of the polymer scaffold, increasing the elastic modulus of the corresponding gels. Multi-arm PEGs contribute additional crosslinking points to gel formation independently of the crosslinking reaction, which is useful in case of sluggish conversion of functional end groups. A comparison of the SCPs made from these different PEGs reveals the impact of PEG molecular weight and architecture on the mechanical properties. For step-growth-polymerized gels, two different 2 kDa four-arm PEGs were chosen. The crosslinking relies on a thiol-Michael addition. Maleimides are used as the ene component due to their superior reactivity with thiols compared to e.g. acrylamides and acrylates. The reaction rate is typically adjusted by varying pH and buffer concentration.

A second focus of this study is the functionalizability of SCPs, as this is a prerequisite for performing biosensing assays. Strategies for the introduction of groups for later coupling reactions include post-synthesis grafting of small unsaturated molecules with carboxy groups. This method allows superior control over the density of the functional groups on the SCPs and the carboxy groups without compromising the mechanical properties of the SCPs. As a drawback, several additional steps to introduce these functional groups are necessary [7]. In addition, a one-

step procedure for gel formation and functionalization is probed by using molecules bearing photocrosslinkable acrylamide groups as well as carboxy groups for further coupling reactions. This approach is convenient, but the bifunctional molecules for functionalization consume potential crosslinking sites, leading to a decrease in elastic modulus, which must be compensated. As a third option, groups that were not reacted during the crosslinking reaction are tested for their usefulness as functionalization sites. Therefore, unreacted groups were functionalized with bifunctional small molecules, since these are commercially available and inexpensive with a large variety of functional groups. In this context, thiol-Michael addition was used for gels prepared by both chain-growth and step-growth mechanisms since both gels are prepared from precursors containing Michael acceptors. Thiol-Michael additions offer the advantage of high reaction rates with low cross-reactivity and that no other compounds or reagents are required for the coupling.

An overview of all synthesized and functionalized SCPs is provided in **Tab. S1**.

Table S1: Summary of synthesized and functionalized SCPs. Corresponding functionalization method, molecule used for functionalization and the reference are given.

SCP synthesis method	Precursor molecules (PEG)	Functionalization	Functionalization method	Compound for functionalization	reference/section
Photoradical	0.3 kDa linear PEG-diacrylamide	-			SCP synthesis based on PEG-ACA and functionalization by photoradical grafting, (Fig. 1)
		COOH	photoradical grafting	crotonic acid	
	3.7 kDa linear PEG-diacrylamide	-			
		COOH	photoradical grafting	crotonic acid	
	2 kDa four-arm starPEG acrylamide	-			Functionalization of SCPs based on starPEG-ACA by thiol-Michael addition, (Fig. 2)
		OH	thiol-Michael addition	mercaptoethanol	
		NH_2		cysteamine	
		COOH		thioglycolic acid	
		SH		ethanedithiol	
				hydrogen sulfide	S8, ESI
		I, SH II, COOH	thiol-Michael addition (both steps)	I, ethanedithiol II, maleimidopropanoic acid	Functionalization of SCPs based on starPEG-ACA by thiol-Michael addition (Fig. 3)
		I, SH II, NH_2		I, ethanedithiol II, maleimidoethylamine	
		COOH	during particle synthesis	2kDa linear acrylamide-PEG-COOH	S3, ESI
		I, COOH II, NH_2	I, during particle synthesis (COOH) II, active ester (NH_2)	I, 2kDa linear acrylamide-PEG-COOH II, ethylenediamine	
Thiol-Michael addition	2 kDa four-arm starPEG maleimide + 2 kDa four-arm starPEG thiol	-			Microfluidic SCP synthesis and functionalization based on starPEG-SH and starPEG-mal (Fig. 4)
		COOH	thiol-Michael addition	thioglycolic acid	
				maleimidopropanoic acid	
		biotin		biotinyl-PEG_2-maleimide	S10, ESI
		I, biotin II, streptavidin	I, thiol-Michael addition II, affinity binding	I, biotinyl-PEG_2-maleimide II, streptavidin	
		streptavidin	thiol-Michael addition	SMCC conjugated streptavidin	

S3. SCP synthesis based on photocrosslinkable PEG–ACA and functionalization by photoradical grafting during synthesis

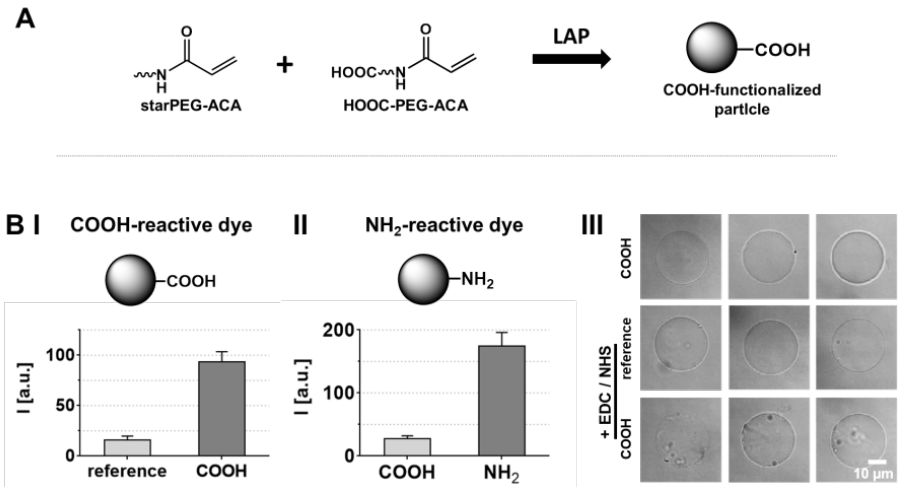

Figure S2: Simultaneous synthesis and COOH-functionalization of SCPs made from starPEG-ACA generated by photoradical reactions. A, Overview of PEG macromonomers (2 kDa starPEG-ACA and 2 kDa ACA-PEG-COOH) and reaction scheme. UV-initiated crosslinking of the PEG-ACA end groups leads to covalent anchoring of the COOH-bearing PEG derivative to the polymer scaffold by the same photoradical coupling reaction used for macromonomer crosslinking. **B I,** Verification of SCP-functionalization based on the comparison of fluorescence intensities via cLSM. COOH-groups of the particles were stained with COOH-reactive FAM-NH_2 by active ester chemistry (EDC/NHS) and analyzed via cLSM to verify the presence of COOH-groups. **II,** Ethylenediamine is coupled to COOH-functionalized SCPs by active ester chemistry (EDC/NHS), stained with amine-reactive FITC and analyzed via cLSM to verify the presence of NH_2-groups after ethylenediamine functionalization. **III,** Bright-field images of COOH-functionalized SCPs before and after treatment with EDC/NHS as well as SCPs made from starPEG-ACA (2 kDa) as a reference. Degradation of SCPs is exclusively observable in the case of COOH-functionalized SCPs treated with EDC/NHS (bottom row). 20 SCPs per condition were measured for cLSM and bright-field analysis. Results are presented as mean + SD.

S4. Optimization of double bond conversion and mechanical properties of SCPs based on photocrosslinkable starPEG-ACA

To minimize the impact of remenant double bonds after SCP synthesis based on photocrosslinkabe starPEG-ACA on post-synthesis functionalization approaches, we closely examined and optimized synthesis parameters. Here, we started with an improvement of double bond conversion by adjusting solid content, photoinitiator concentration as well as irradiation time and intensity. To test the dependence of SCP contact area on the tested parameters, SCPs were applied to glass slides cleaned with isopropanol (Applichem, Germany) in an ultrasonic bath. These surfaces possess sufficient hydrophobicity to drive entropic adhesion of SCPs. SCPs

synthesized using flow rates of Q_d = 50 µL h^{-1} and Q_C = 200 µL h^{-1} revealed only minor differences in diameter (24.4 ± 1.0 µm (5% (w/w), 24.2 ± 1.0 µm (7.5% (w/w) and 22.6 ± 0.6 µm (10% (w/w)), making RICM a suitable method to compare contact radii and indirectly particle stiffness (see **eq. 1**).

As expected, contact areas of SCPs adhering to unfunctionalized glass surfaces decreased with increasing PEG solid content, indicating higher elastic moduli for higher solid contents (**Fig. S3 A I**). It has to be noted that SCPs made from 5% (w/w) PEG solutions yielded blurred, non-circular interfacial areas and a lack of Newtonian fringes, making this type of SCP unsuitable for precise measurements. RICM images of SCPs made from 7.5 and 10% (w/w) PEG solutions showed strong contrast and circular contact areas. The SCP stiffness could be further increased by using higher concentrated PEG solutions above 10% (w/w) (see **ESI section 5, Fig. S4**). However, follow-up experiments were conducted with SCPs made from 10% (w/w) PEG solutions, as SCPs with higher elastic moduli resulted in smaller contact areas and consequently lower sensitivity in subsequent sensing applications. Additionally, higher concentrated PEG solution exhibit increased viscosity, which might lead to non-uniform SCPs and satellite droplet formation. A slight difference between unfunctionalized and COOH-functionalized SCPs could be observed, indicating either the presence of attractive interactions between SCPs and the glass surface or negligible alterations of elastic moduli after COOH-functionalization.

Next, the effect of photoinitiator concentration on the double bond conversion of the SCPs was examined. Photoinitiator contents ranging from 1 to 4% (w/w) were tested. Increasing the concentration from 1 to 2% (w/w) resulted in smaller contact areas for both unfunctionalized and COOH-functionalized SCPs (**Fig. S3 A II**). A further increase above 2% (w/w) resulted in larger contact radii, most likely due to chain terminations caused by the increased amount of photoinitiator radicals in higher concentrated solutions. The photoinitiator concentration for subsequent experiments was therefore set to the optimum concentration of 2% (w/w). In addition to the aforementioned synthesis parameters, the irradiation time was optimized. Freshly synthesized SCPs were UV-irradiated (254 nm) for 0.5 to 3 min, and contact radii were analyzed by RICM. As can be seen from **Fig. S3 A III**, the SCP stiffness (i.e. the decrease in the contact area) correlates with the exposure time, with saturation being reached after 3 minutes of UV exposure.

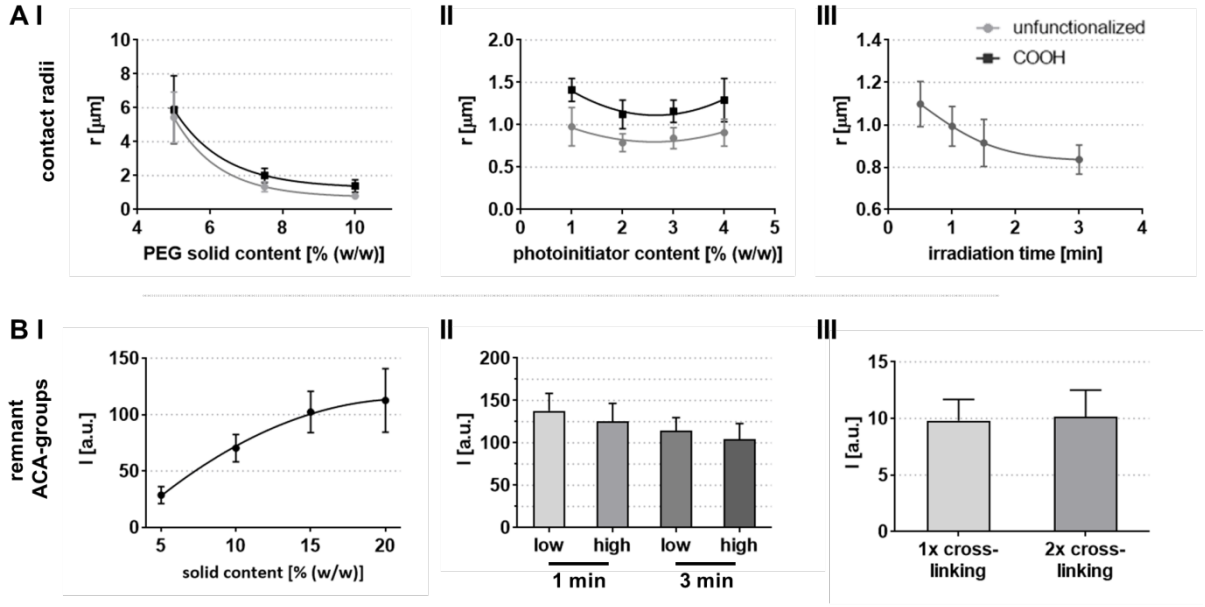

Figure S3: Analysis and optimization of synthesis and functionalization parameters of SCPs made from 2 kDa starPEG-ACA (Q_d = 40 µL h^{-1}, Q_C = 400 µL h^{-1}). **A,** The impact of synthesis parameters on the mechanical properties of SCPs was probed by contact area analysis using RICM. SCPs with a lower elasic modulus are characterized by the formation of increased contact radii. **I,** Analysis of contact radii in dependence on PEG solid content at 1% (w/w) photoinitiator concentration. **II,** Contact radii in dependence on photoinitiator concentration (10% (w/w) PEG). **III,** Contact radii in dependence on UV irradiation time (10% (w/w) PEG, 2% (w/w) photoinitiator). The graphs for non-functionalized and functionalized SCPs are indicated by grey and black lines, respectively. SCPs adhered to uncoated glass surfaces. Mean contact radii of at least 50 particles per condition are shown except for SCPs made from 5% (w/w) PEG solutions. In this case, the mean contact radius of 10 SCPs is presented. Error bars indicate SD. **B,** Determination of remnant ACA-groups of FITC-labeled unfunctionalized SCPs by cLSM. Fluorescence intensity increases with an increasing number of remnant ACA-groups. **I,** Variation of the solid content of the PEG solutions between 5 and 20%. The number of remaining ACA-groups correlates positively with the solid content. **II,** Impact of UV intensity and irradiation time. Both correlate positively with double bond conversion. The low and high irradiation intensity represents a curing setup with five 8 W UV lamps (low) and a 250 W (high) UV lamp, respectively. **III,** Impact of a repeated crosslinking step after initial crosslinking and workup. Photoinitiator was added to an SCP suspension and irradiated. Both crosslinking steps were conducted using a curing setup with five 8 W UV lamps and an irradiation time of 3 minutes. The photoinitiator content used for all SCP syntheses depicted in b was 2% (w/w). At least 20 particles per condition were fluorescently labeled and measured via cLSM. Results are presented as means and error bars indicate SD.

It should be noted that confinement of polymer precursor molecules at high w/w content within the comparatively small droplet volume generated by the microfluidic flow-focusing device is associated with a steric hindrance that severely limits the mobility of the reactive species during crosslinking. Hence, unreacted functional ACA-residues are most likely present in the resulting particles, as reported in previous studies [13]. We therefore exploited fluorescein isothiocyanate (FITC) for labeling these remnant groups. As can be seen from **Fig. S3 B I**, the number of available ACA-groups increased strongly with the PEG macromonomer solid content. A similar series of experiments with mixtures of linear and starPEG macromonomers did not reveal options

for a comprehensive improvement of double bond conversion or a reduction of the remnant functional groups (see **ESI section 6, Fig. S5**). The addition of highly mobile monofunctional small molecules to quench the remnant groups was not tested at this point, as this strategy is expected to excessively reduce the elastic moduli. Therefore, we investigated the impact of UV irradiation time as well as intensity on the number of remnant ACA-groups using a low (5 x 8 W, 43 mW cm^{-2}) and a high energy (250 W, 250 mW cm^{-2}) UV curing device to exclude possible consequences of oxygen inhibition due to rapid diffusion of gas into the solution. Only a minor improvement could be achieved by increasing the UV intensity, whereby the same UV irradiation time dependence could be observed for both setups (**Fig. S3 B II)**. Prolonged irradiation at high intensity yields clumped and irregularly shaped SCPs (data not shown). Finally, to verify that the maximum double bond conversion for the 2 kDa starPEG-ACA system was achieved, we followed up with a second crosslinking step, i.e. the addition of photoinitiator to cured and fully swollen SCPs. As no difference in fluorescence intensity in comparison to the reference (1x crosslinking) could be detected, it was concluded that no further improvements regarding double bond conversion are possible (**Fig. S3 B III**).

S5. Impact of PEG solid content on contact radii of SCPs based on photocrosslinkable starPEG-acrylamides

For synthesis of SCPs made from 2 kDa 4-arm-starPEG-acrylamide (starPEG-ACA), 10, 15 and 20% (w/w) PEG solutions were prepared and lithium phenyl-2,4,6-trimethylbenzoylphosphinate (LAP) was added in a concentration of 2% (w/w). Generation of droplets, synthesis of SCPs and workup was performed as described in the Experimental section.

The radius of contact and the modulus of elasticity of SCPs are important parameters that influence the performance of the sensor and allow adjusting the working range and sensitivity of the sensor. Hence, the influence of 2 kDa starPEG-ACA solid content on contact radii of the SCPs was investigated (see **Fig. S4**). By increasing the PEG solid content, the contact radii decreased without affecting the radius of the SCPs, which indicates increasing elastic moduli with increasing PEG solid contents. SCPs made form PEG solutions containing more than 20% (w/w) PEG were not investigated, as solutions containing 10% (w/w) PEG proved to yield the most suitable SCPs for our purpose.

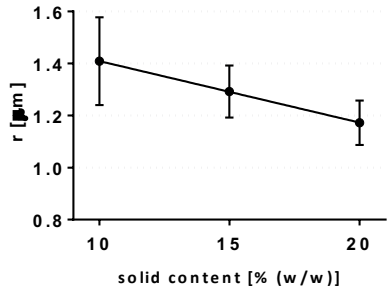

Figure S4: Analysis of contact radii of SCPs made from 10, 15 and 20% (w/w) solutions of 2 kDa starPEG-ACA. SCPs adhered to uncoated glass surfaces and were evaluated using RICM. Mean contact radii of at least 50 particles per condition are shown. Error bars indicate SD.

S6. Microfluidic preparation and characterization of SCPs made from mixed linear and star-shaped PEGs

For the synthesis of SCPs made from mixtures of 0.3 kDa acrylamide-PEG-acrylamide (ACA-PEG-ACA) and 2 kDa starPEG-ACA, 10% (w/w) PEG (total PEG concentration) solutions containing different ratios of ACA-PEG-ACA and starPEG-ACA in ultrapure water were prepared, and LAP was added in a concentration of 2% (w/w). Generation of droplets, synthesis of SCPs and workup was performed as described in the Experimental section.

In addition to the optimization of the synthesis parameters of SCPs made from 2 kDa starPEG-ACA, the impact of the addition of 0.3 kDa linear ACA-PEG-ACA on double bond conversion was assessed. Therefore, mixtures with a total solid content of 10% (w/w) PEG were prepared as precursor solutions. Low molecular weight (0.3 kDa) linear starPEG exhibits higher diffusivity than its starPEG counterpart, which is likely to be associated with improved conversion rates of acrylamide- (ACA) groups. With two ACA-groups present on the 0.3 kDa linear PEG, the molecule has two possible residues that can each form two radicals for crosslinking, whereby the same mass of 0.3 kDa ACA-PEG-ACA has roughly three times more ACA-groups than 2kDa starPEG-ACA.

However, increasing the percentage of linear ACA-PEG-ACA did not lead to more strongly crosslinked particles and the contact areas increase with increasing proportions of the linear ACA-PEG-ACA, indicating lower elastic moduli (**Fig. S5 B**). Fluorescence intensities of the FITC-labeled SCPs serve as a measure of remnant ACA-groups, i.e. ACA-groups not involved in the crosslinking reaction. As can be seen from **Fig. S5 B**, fluorescence intensities positively

correlate with the amount of linear ACA-PEG-ACA added. SCPs made exclusively from ACA-PEG-ACA exhibit three times the fluorescence intensity compared to SCPs made exclusively from starPEG-ACA. None of the results suggests any improvement of SCP-crosslinking. Mixed linear and star-shaped PEG systems were therefore not taken into further consideration.

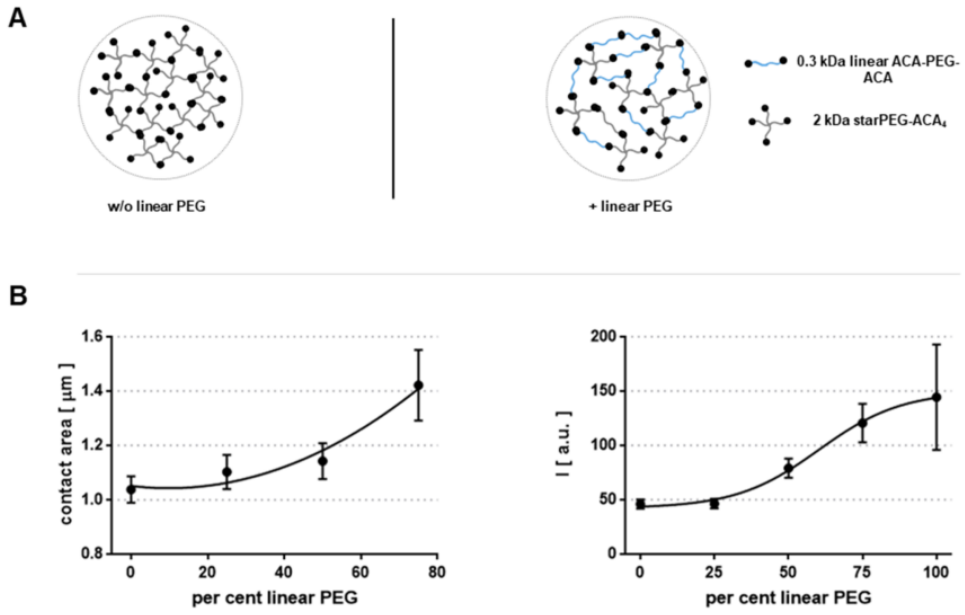

Figure S5: Analysis and optimization of synthesis parameters of SCPs made from mixed PEG system containing 2 kDa starPEG-ACA and 0.3 kDa linear ACA-PEG-ACA. A, Schematic representation of the optimization strategy based on a mixed PEG system with different percentages of 0.3 kDa linear ACA-PEG-ACA (blue) and 2 kDa starPEG-ACA (black). Left: SCP made from 2 kDa starPEG-ACA. Right: SCP made from 2 kDa starPEG-ACA plus 0.3 kDa linear ACA-PEG-ACA. **B,** Contact radii and fluorescence intensities of SCPs in dependence of the proportion of 0.3 kDa linear PEG (10% (w/w) total PEG solid content). Left: Contact radii of SCPs adhering to uncoated, cleaned glass surfaces. Right: Fluorescence intensities of FITC-stained SCPs measured by cLSM. Results are presented as means and error bars indicate SD.

S7. Single particle homogeneity assessment of functionalized SCPs based on photocrosslinkable 2 kDa starPEG-ACA

SCPs were synthesized as described in the Experimental section. Solutions containing 10% (w/w) 2 kDa starPEG-ACA and 2% (w/w) LAP were used.

For homogeneity assessment of SCPs, bright-field images were acquired as described in **ESI section 14** and analysis was conducted using Fiji software [14]. For single particle analysis of homogeneity, a linear section within one particle per condition was examined. Therefore, a grey

value profile was plotted, and the minimum value obtained from each condition was regarded as background and subtracted from all values obtained within the respective condition. The resulting maximum value within a test series (several conditions) was defined as 100% grey value intensity and the scale was divided into 5% quantiles. The frequency distribution of the values within the quantiles was plotted and fitted using Gaussian distribution. Curve fitting was conducted using GraphPad Prism (GraphPad Software, US).

To compare averaged grey value standard deviations, the standard deviation of 15 linear sections within 5 SCPs per condition was averaged and plotted as a function of functionalization degree.

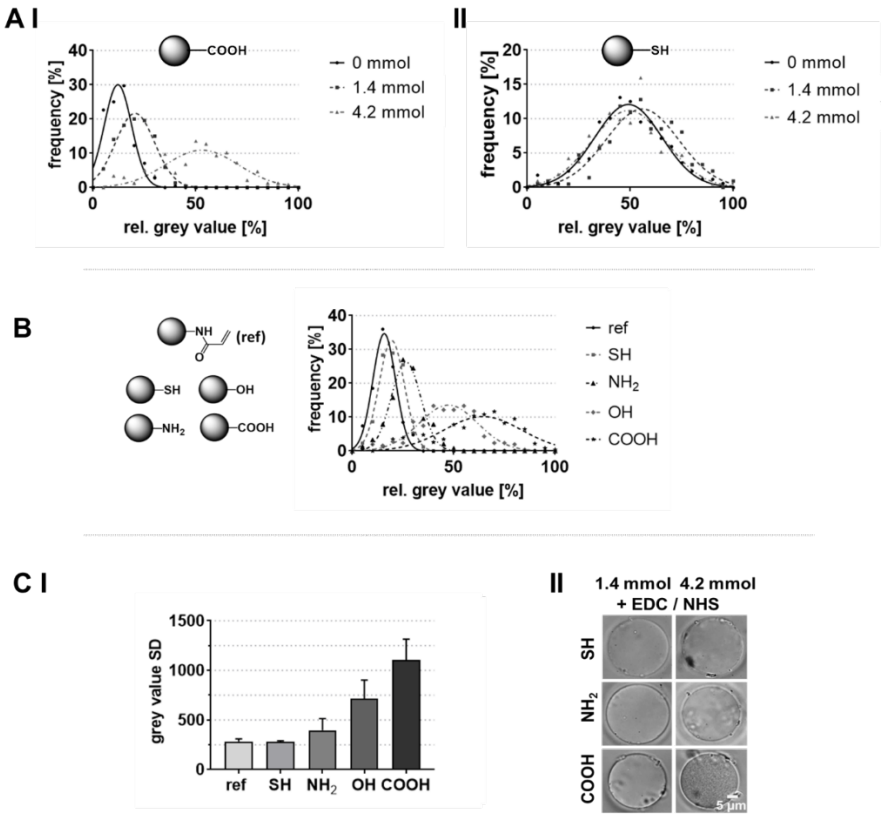

Figure S6: Characterization of functionalized SCPs made from 2 kDa starPEG-ACA by grey value analysis. A, Single particle analysis of grey value distribution of unfunctionalized (0 mmol) SCPs and SCPs functionalized with 1.4 or 4.2 mmol of thioglycolic acid (**I**) and ethanedithiol (**II**). **B,** Single particle analysis of grey value distribution of all types of SCPs functionalized with 4.2 mmol of the respective thiol compound. SCPs were functionalized with ethanedithiol (SH), cysteamine (NH_2), mercaptoethanol (OH) and thioglycolic acid (COOH). **C,** Comparison of averaged grey value standard deviations of all types of SCPs (**I**) and representative bright field images of SCPs suffering from degradation caused by EDC/NHS activation at low (1.4 mmol) and quantitative (4.2 mmol) functionalization (**II**). For analysis of averaged grey value standard deviations, 5 SCPs per condition, each at 3 different regions, were measured. Results are presented as means and error bars indicate SD.

S8. Thiol-functionalization and characterization of SCPs based on photocrosslinkable 2 kDa starPEG-ACA using hydrogen sulfide

SCPs were synthesized as described in the Experimental section. Solutions containing 10% (w/w) 2 kDa starPEG-ACA and 2% (w/w) LAP were used. Thiol- (SH) functionalization of SCPs employing ethanedithiol was conducted as described in the Experimental section.

As an alternative approach for introducing SH-groups, hydrogen sulfide (H_2S) was coupled to unreacted residual ACA-moieties within the PEG network employing thiol-Michael addition. 5 mL of the SCP suspension was centrifuged at 1850x g, the supernatant was discarded, and the SCPs were subsequently resuspended in 5 mL HEPES buffer. 5 mL of a 0.8 M H_2S solution in THF (Sigma Aldrich, US) were mixed with 10 mL HEPES buffer and the pH was adjusted to 7.0. After combining the SCP suspension and H_2S-solution, the reaction was allowed to proceed for 1 h while agitating. Subsequently, the suspension was centrifuged, the supernatant was discarded, and the SCPs were washed five times with HEPES buffer.Functionalization of H_2S-functionalized SCPs bearing SH-groups was conducted employing maleimide (mal) compounds. Therefore, alpha-maleimido-24(ethylene glycol)-omega-propionic acid (mal-PEG_{24}-COOH, Iris Biotech, Germany) was dissolved in 100 mM HEPES buffer in a concentration of 10, 20 and 30 mg mL^{-1}, and the pH was adjusted to 7.0 by adding of NaOH. The suspension containing SH-functionalized SCPs was split into 1.5 mL fractions, centrifuged at 1840x g, the supernatant was discarded, and 1.5 mL of the respective solution was added to the SCP pellet. The reaction was allowed to proceed for 1 h while agitating. Subsequently, the SCPs were centrifuged and rinsed at least three times with 100 mM HEPES buffer.

The SCPs were labeled with *N*-(5-fluoresceinyl)maleimide (FAM-mal) as described in the Experimental section. Homogeneity assessment was conducted as described above (**ESI section 7**) and in the Experimental section.

Fig. S7 provides a comparison of SCPs based on 2 kDa starPEG-ACA functionalized with ethanedithiol and hydrogen sulfide. Both strategies yield SH-functionalized SCPs. The efficiency of SH-group introduction was probed using FAM-mal for SH-staining and cLSM for fluorescence intensity measurements of the labeled SCPs. Ethanedithiol-functionalized SCPs exhibit roughly twice the fluorescence intensity of H_2S-functionalized SCPs, indicating a higher functionalization degree (**Fig. S7 A**, left). It has to be noted that functionalization employing ethanedithiol was conducted with 1.25-fold the amount of substance compared to H_2S-functionalization. To verify SH-functionalization, mal-PEG_{24}-COOH was coupled to SCPs

functionalized with hydrogen sulfide and residual SH-groups were labeled with FAM-mal. Quantitative conversion of SH-groups was achieved by the addition of a 10 mg mal-PEG_{24}-COOH solution per 1 mL of the SCP suspension, as can be seen from **Fig. S7 A** (right).

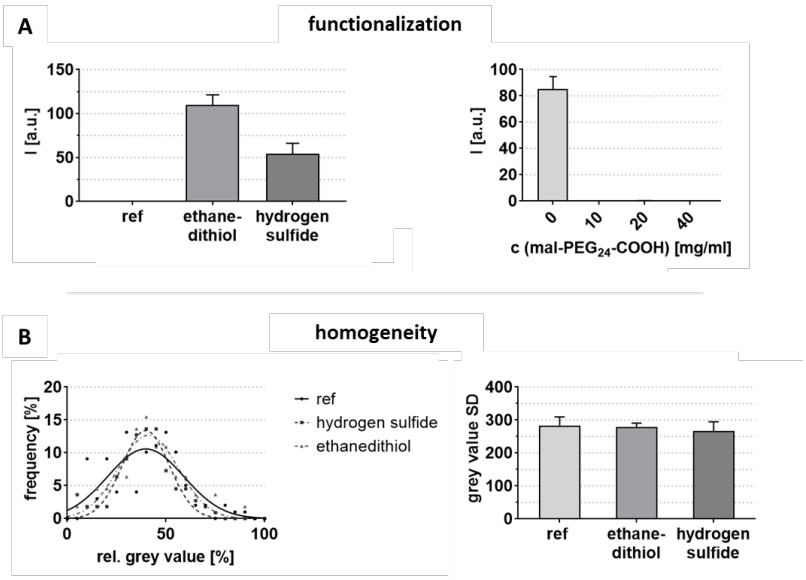

Figure S7: Characterization of SH-functionalized SCPs made from 2 kDa starPEG-ACA by cLSM and particle grey value analysis. A, Comparison of fluorescence intensities of FAM-mal-stained SCPs by means of cLSM. Left: Comparison of SCPs functionalized with ethanedithiol to SCPs functionalized with hydrogen sulfide. Unfunctionalized SCPs served as a reference. Right: mal-PEG_{24}-COOH was coupled to H_2S-functionalized SCPs. Concentration dependent conversion of SH-groups was probed by FAM-mal labeling of residual SH-groups. **B,** Homogeneity assessment of unfunctionalized SCPs and SCPs functionalized with ethanedithiol or hydrogen sulfide by grey value analysis. Left: Single particle analysis of grey value distributions. Right: Comparison of averaged grey value standard deviations. For all fluorescence-based analysis of SCPs, 60 particles per condition were measured. For homogeneity assessment by comparison of grey value SD, 5 SCPs per condition, each at 3 different regions, were measured. Results are presented as means and error bars indicate SD.

The effect of both SH-functionalization approaches on particle homogeneity was assessed by single particle analysis of grey value distribution. The grey value distributions for both types of SH-functionalized SCPs exhibit impeccable overlap with the reference (unfunctionalized SCP), thereby indicating the absence of degradation effects (**Fig. S7 B** left). To assure an adequate averaging over several SCPs, the standard deviation of 15 sections was calculated and utilized as a measure of homogeneity. As depicted in **Fig. S7 B** (right), none of the functionalized SCPs exhibit significant differences in grey value standard deviation compared to the reference, verifying the absence of degradation effects.

S9. Preparation of streptavidin-coated glass surfaces

For the preparation of biochip surfaces, glass coverslips (Menzel Glaeser, Ø 32 mm, Thermo Fisher Scientific, US) were pre-cleaned in ultrapure water and ethanol for 30 min each. A chemical cleaning process was performed subsequently in a mixture of ultrapure water, 25% (v/v) NH_3 aqueous solution (Merck, Germany) and 35% (v/v) H_2O_2 (Grüssing, Germany) in a ratio of 5:1:1 for 10 min at 64 °C. After rinsing twice with ultrapure water, the coverslips were dried in a nitrogen stream. The coverslips were then silanized with 3-aminopropyl)triethoxysilane **(**APTES, 0.51% (v/v), Sigma Aldrich, US) dissolved in isopropanol with 1.1% (v/v) ultrapure water for 10 min with continuous stirring, washed twice with isopropanol and dried again in a nitrogen stream. Annealing of the silanized coverslips was carried out in an oven at 120 °C for 1 h.

To coat the silanized glass surfaces with poly(ethylene-alt-maleic anhydride) copolymer (PEMA, average Mw = 100,000 – 500,000 g mol^{-1}, Sigma Aldrich, US), 100 µL of a solution of 0.1% (w/v) PEMA dissolved in a 1:2 acetone-THF mixture were centrally pipetted on the coverslips. A spin coating process was used to produce a thin and evenly distributed layer of PEMA. Immediately after the polymer solution was pipetted onto the glass surface, the coverslip was slowly rotated for 1 s so that the liquid could homogeneously cover the surface. This first acceleration step was followed by a maximum rotation step of 3000 rpm for 30 s. In order to stabilize the linkage between the silanized glass surface and PEMA, the coverslips were then annealed at 120 °C for 2 h, as described above. Excess polymer was removed by leaving the coverslips in acetone for 15 min, followed by washing each sample three times with acetone before drying them in a nitrogen stream.

To produce streptavidin- (SA) coated glass surfaces, freshly annealed PEMA-coated glass slides presenting amine reactive anhydrides were covered with 1.5 mL of a 1 mg mL^{-1} SA-solution in 100 mM HEPES buffer, pH = 7.0. After 60 min incubation at room temperature, the surfaces were washed several times with 100 mM HEPES buffer, pH = 7.0 for further use to carry out interaction studies between biotin-functionalized SCPs and SA-coated surfaces.

The success of functionalization and coupling reactions was assessed by cLSM. For the introduction of fluorescent moieties, biotin-4-fluorescein (FAM-btn), which specifically binds to SA, was used. 250 µg mL^{-1} of FAM-btn was weighed and dissolved in 100 mM HEPES buffer (pH = 7.0). 2 mL of the staining solution was pipetted onto the coated coverslips and the reaction was allowed to proceed overnight. Finally, the supernatant was discarded, and the coverslips were washed several times in 100 mM HEPES buffer (pH = 7.0).

Fig. S8 illustrates the covalent immobilization of SA on PEMA-coated transparent coverslips. The carboxylic anhydride residues form a stable amide bond upon reaction with NH_2-groups of SA. The tetrameric structure of SA ensures the presence of accessible binding sites for biotin. SA-immobilization was verified by means of cLSM. Therefore, PEMA-coated surfaces (reference) as well as SA-coated surfaces were stained using FAM-btn. Strong fluorescence was observed in the case of SA-coated surfaces, whereas the reference surfaces showed neglectable fluorescence intensities, thereby indicating successful immobilization of SA.

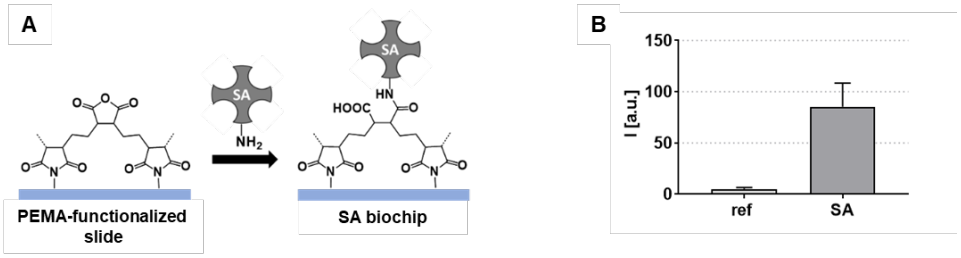

Figure S8: SA-coating of coverslips. A, Illustration of immobilization of SA using a PEMA-coated surface. PEMA bears carboxylic anhydrides, capable of forming amide bonds with the amino groups of SA. **B,** Verification of SA-immobilization by cLSM. FAM-btn-labeled PEMA- and SA-coated surfaces were compared. 15 patches on 3 coverslips per condition were measured. Results are presented as means and error bars indicate SD.

S10. Biotin and streptavidin conjugation of SCPs based on thiol-Michael addition of starPEG-SH and starPEG-mal

To investigate the suitability of this functionalization strategy for SCP conjugation with relevant amine-bearing targets, we used the biotin (btn) - streptavidin (SA) model system to its easy availability and the specific interaction. Three conjugation strategies were tested: direct btn-functionalization of SCP using biotinyl-PEG-maleimide (mal-btn); indirect SA-functionalization of SCP by coupling SA to btn-functionalized SCPs and direct SA-functionalization of SCPs via maleimide activated SA (**Fig. S9 A**). For the later case a low molecular excess of

sulfosuccinimidyl 4-(N-maleimidomethyl)cyclohexane-1-carboxylate (s-SMCC), presenting an activated COOH-group for SA-coupling and a mal-group for tethering the conjugate to SCPs in a subsequent step. SA-immobilization was verified via labelling of the binding pockets with biotin-4-fluorescein (FAM-btn). Details of the preparation are specified below.

The strategies indicated very efficient coupling of btn and SA to SCPs and no visible degradation effects (**Fig. S9 B**). Besides this straightforward verfication of the functionalizability of starPEG-SH/mal SCPs it has to be mentioned that the investigated btn- and SA-conjugated SCPs can serve as a platform for convenient binding of various molecules of interest to SCPs using the SA-btn system.

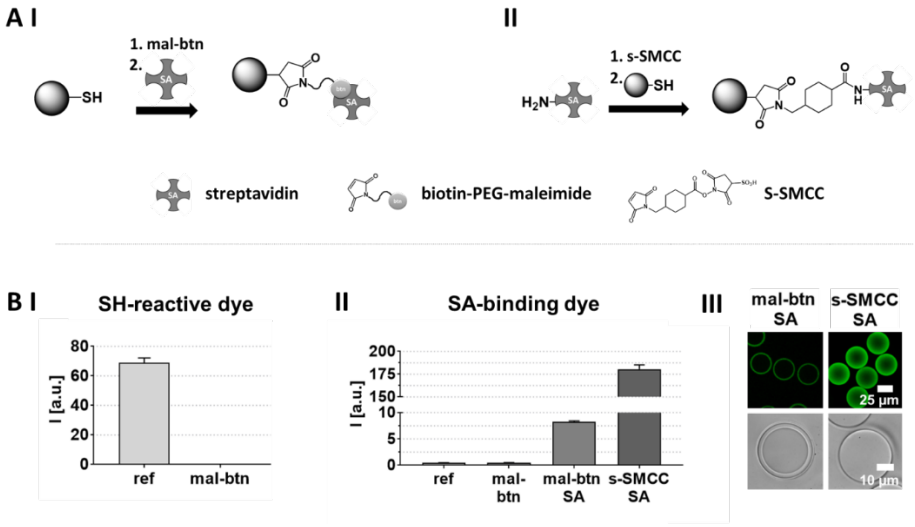

Figure S9: SCP conjugation strategies based on starPEG-SH/-mal using maleimides. A, Overview of functionalization strategies. **I,** Biotinyl-PEG_2-maleimide (mal-btn) is coupled to SCPs bearing SH-groups using thiol-maleimide addition. Subsequently, SA is tethered to the biotin-functionalized SCPs using affinity binding. Tetravalency of SA assures the presence of unoccupied binding pockets of the immobilized protein. **II,** Sulfosuccinimidyl 4-(N-maleimidomethyl)cyclohexane-1-carboxylate (s-SMCC) is coupled to an NH_2-group of SA for introducing mal-groups in a first step. In a second step, the mal-functionalized SA is added to a suspension of SCPs bearing SH-groups, and immobilized on the SCPs using thiol-maleimide addition. **B I,** Proof of mal-btn-coupling using FAM-mal labeling and cLSM analysis. SH-groups are quantitatively converted, resulting in weakly fluorescent SCPs. **II,** SA-immobilization was probed using affinity binding of biotin-4-fluorescein (FAM-btn) to SA decorated SCPs and cLSM analysis. Strong fluorescence is exclusively detectable for SA functionalized SCPs, with SA immobilization using s-SMCC yielding the highest fluorescence intensity and therefore highest SA density. **III,** Micrographs showing the appearance of SA-functionalized SCPs were recorded by cLSM (top) and bright-field microscopy (bottom). Annular structures are formed in the case of the mal-btn functionalization strategy, while no such effect is observed for the s-SMCC functionalization strategy. Please note that only cross-sections in close proximity to the SCP-glass surface interface were measured to obtain fluorescence intensities in these homogeneously labeled regions. Fluorescence intensities were calculated from 60 particles per condition. Results are presented as means +SD.

Preparation of biotin-functionalized SCPs

For the studies of interaction and adhesion of biotin-functionalized SCPs on streptavidin- (SA) coated glass surfaces, SCPs made from a 10% (w/w) solution of starPEG-mal and starPEG-SH were used. 1 mL of the SCP suspension was centrifuged at 1844x g for 10 min and the supernatant was discarded. SCPs were functionalized with biotin by adding 1 mg mL^{-1} of biotinyl-PEG_2-maleimide (Bachem, Switzerland) dissolved in 100 mM HEPES buffer (pH = 7.0) to the particles. The reaction was allowed to proceed for 1 h while agitating, followed by three washing steps.

Preparation of streptavidin-functionalized SCPs

Two different strategies were employed to functionalize SCPs with streptavidin (SA). The first strategy utilizes biotin-coated SCPs (see above) and the biomolecular recognition between biotin and SA. Therefore, 1.3 mL of a solution containing 1 $mgmL^{-1}$ SA (ProSpec-Tany TechnoGene, Israel) in 100 mM HEPES buffer (pH = 7.0) was prepared. 500 µL of a suspension containing biotin-functionalized SCPs was centrifuged, 300 µL of the supernatant was discarded, and the SCPs were subsequently resuspended in the SA solution. After 1 h of incubation while agitating, the SCP suspension was centrifuged again and washed at least three times with 100 mM HEPES buffer.

For coupling via sulfosuccinimidyl 4-(N-maleimidomethyl)cyclohexane-1-carboxylate (s-SMCC, Iris Biotech, Germany), 1.5 mL of a 400 nM s-SMCC solution in 100 mM HEPES buffer was prepared. Subsequently, 1.5 mg of SA were dissolved in the solution and allowed to react for 30 minutes at room temperature. Meanwhile, 500 µL of a suspension containing unfunctionalized SCPs made from 10% (w/w) 2 kDa starPEG-mal and starPEG-SH was centrifuged, and 300 µL of the supernatant was discarded. 1.3 mL of the solution containing the activated SA was added to the SCPs and left for 1 h. Finally, the suspension was centrifuged and washed three times with 100 mM HEPES buffer.

S11. Microfluidic device fabrication

A combination of photo and soft lithography was used for the preparation of poly(dimethylsiloxane) (PDMS)-based flow-focusing microfluidic devices. Silicon wafers containing a defined microstructure with a channel height of 10 and 25 µm, serving as a negative master, were prepared as follows: First, a negative photoresist (SU-8 25, Microchem. Co., Westborough, MA, US) was spin-coated onto a 3-inch silicon wafer (Siegert Wafer, Aachen, Germany). Patterning of the silicon wafer with the desired microchannel structure was achieved by UV-illumination of the photoresist through a printed photomask using a mask aligner (MJB3, Süss MicroTec, Garching, Germany). Subsequent removal of non-illuminated photoresist by washing with a developer solution (mr-Dev 600, Micro Resist Technology, Berlin, Germany) yielded the desired microchannel structure with defined height and width. After cleaning with filtered isopropanol, a degassed solution of PDMS base and crosslinker (DOWSIL™ 184 Silicone Elastomer Base, Dow, US) in a ratio of 10:1 was poured onto the silicon wafer, repeating the degassing step once for 30 minutes before curing at 65 °C for 2 h. The device was cut out with a scalpel, and access ports for tubing (1 mm) were punched into the device with a biopsy needle (Ø 1 mm, pfm medical). The microfluidic device was then assembled by bonding the PDMS replica to a cleanroom-cleaned glass slide (Schott Nexterion, Germany), treated with oxygen plasma in a low-pressure plasma chamber (PDC-002, Harrick Plasma, US) immediately before bonding. PDMS replica and glass slides form stable Si-O-Si bonds when brought into contact after plasma treatment. Finally, the microfluidic channels were treated with 1% (w/w) tridecafluoro-1,1,2,2-tetrahydrooctyl-trichlorosilane (abcr, Germany) in a fluorinated oil (HFE 7500, 3M, US) at room temperature for 1 h and rinsed with HFE 7500 in order to provide a hydrophobic surface for ideal flow conditions.

S12. Fluorescence microscopy of SCPs

Successful functionalization was assessed employing confocal laser scanning microscopy (cLSM, LSM700, Zeiss, Germany). Therefore, untreated coverslips (Ø 32 mm, Menzel Glaeser, Thermo Fisher Scientific, US) were adhered to a sticky-slide 16 well (Grace Biolabs, US), and each surface was covered with 200 µL of 100 mM HEPES buffer (pH = 7.0). 50 µL of the respective SCP suspension was carefully pipetted into the wells, allowed to sediment for 20 min, and the particles were subsequently investigated. With the exception of TAMRA-scm-stained SCPs, all

stained samples were excited using a 488 nm solid-state laser. TAMRA-scm was excited using a 555 nm solid-state laser. Stained SCPs were imaged using a C-Apochromat water immersion objective with a 40x magnification and a numerical aperture of 1.2 (C-Apochromat 40x/1.20 W Korr, Zeiss, Germany). Areas of 320 x 320 µm (512 x 512 pixels, 1.60 pixels μm^{-1}) were recorded, whereby the z-position of the imaged x-y-plane was individually adjusted to avoid the recording of areas with incomplete staining and gradients from SCP surface to center, respectively. To analyze the fluorescence intensities of the SCPs, the mean grey value of each particle was calculated based on the fluorescence intensity within the corresponding x-y plane using Fiji [14]. Only SCPs located within the central 160 x 160 µm region of each image were analyzed. Unless otherwise stated, 60 SCPs per condition were analyzed.

S13. Bright-field microscopy

SCPs were analyzed using bright-field microscopy to determine whether any defects occurred in the course of synthesis, functionalization, conjugation or activation by active ester chemistry. For imaging, an inverted microscope with an integrated halogen lamp was used (Olympus IX73, Germany). The microscope was equipped with a 60x, NA (numerical aperture) 1.35 oil-immersion objective (UPlanSApo 60x 1.35 oil, Olympus, Germany) and 108.5 x 81.34 µm patches (1600 x 1200 pixel) were imaged using Micro-Manager software [15,16].

S14. Determination of elastic modulus

The Young's modulus of functionalized SCPs was determined by atomic force microscopy (AFM) - based indentation measurements using a NanoWizard IV AFM (JPK instruments, Germany) mounted on an inverted optical microscope (Axio Observer, Zeiss, Germany). Tipless cantilever (PNP-TR-TL-Au, Nanoworld, Switzerland, nominal spring constant k = 0.08 N m-1), equipped with a silica bead (diameter: 10µm, Kisker, Germany) were used for indentation measurements. Cantilever were calibrated by the thermal noise method before each experiment [17]. For indentation measurements, the silica indenter was aligned over the center of individual SCPs and force-distance curves were acquired with an approach velocity of 5 µm/s and a contact force of 2 nN. The Young's modulus of the SCPs was extracted from approach force-distance curves using the Hertz model for spherical indenter and applying a double-contact correction

considering an additional deformation derived from the counter pressure at the bottom side of the bead during indentation.

References

1 D. Pussak, D. Ponader, S. Mosca, S.V. Ruiz, L. Hartmann and S. Schmidt, *Angew. Chem. Int. Ed.*, 2013, **52**, 6084–6087.

2 S. Martin, H. Wang, L. Hartmann, T. Pompe and S. Schmidt, *Phys. Chem. Chem. Phys.*, 2015, **17**, 3014–3018.

3 S. Martin, H. Wang, T. Rathke, U. Anderegg, S. Möller, M. Schnabelrauch, T. Pompe and Schmidt, Polymer, 2016, **102**, 342–349.

4 D. Rettke, J. Döring, S. Martin, T. Venus, I. Estrela-Lopis, S. Schmidt, K. Ostermann and T. Pompe, *Biosens. Bioelectron.*, 2020, **165**, 112262.

5 D. Rettke, F. Seufert, J. Döring, K. Ostermann, D. Wilms, S. Schmidt and T. Pompe, *Biosens. Bioelectron*., 2021, **192**, 113506.

6 D. Pussak, M. Behra, S. Schmidt and L. Hartmann, *Soft Matter*, 2012, 8, 1664–1672.

7 S. Schmidt, H. Wang, D. Pussak, S. Mosca and L. Hartmann, Beilstein J. Org. Chem., 2015, **11**, 720–729.

8 H. Wang, F. Jacobi, J. Waschke, L. Hartmann, H. Löwen and S. Schmidt, *Adv. Funct. Mater*., 2017, **27**, 1702040.

9 L. Limozin and K. Sengupta, *Chemphyschem,* 2009, **10**, 2752–2768.

10 Y. Gao, K. Peng and S. Mitragotri, *Adv. Mater*., 2021, **33**, e2006362.

11 C.C. Lin and K.S. Anseth, *Pharm. Res*., 2009, **26**, 631–643.

12 S. Lee, X. Tong and F. Yang, *Biomater. Sci.*, 2016, **4**, 405–411.

13 S.E. Barnes, Z.T. Cygan, J.K. Yates, K.L. Beers and E.J. Amis, *Analyst*, 2006, 131, 102761033.

14 C.A. Schneider, W.S. Rasband and K.W. Eliceiri, *Nat. Methods*., 2012, **9**, 671–675.

15 A. Edelstein, N. Amodaj, K. Hoover, R. Vale and N. Stuurman, *Curr. Prot. Mol. Biol.* C, 2010, **Chapter 14**, Unit14.20.

16 A.D. Edelstein, M.A. Tsuchida, N. Amodaj, H. Pinkard, R.D. Vale and N. Stuurman, *J. Biol. Meth.*, 2014, **1**, e10.

17 J.L. Hutter and J. Bechhoefer, *Rev. Sci. Instrum.* , 1993, **64**, 1868–1873.